Chapter 8

Polarization shaping of general pulse profiles

In this chapter, a new, unrestricted pulse shaper setup will be discussed in detail. It is able to independently modulate amplitude and phase in two orthogonal directions, and therefore is a full implementation of amplitude, phase, and polarization as it is able to enact the general form of the filter function $\tilde{\mathbf{H}}(\omega)$*. Its description is algebraically simpler, but in return, the experimental effort is costlier as the liquid crystal modulator was incorporated in a Mach-Zehnder interferometer, using wave interferences for controlling the output field. The feasibility to yield single pulses with arbitrary polarization states has already been demonstrated [28]. In this work, the possibilities of generating parametric and arbitrary pulse forms in the time domain are discussed.*

8.1 Parallel setup

8.1.1 Layout

The parallel setup, drawn in Fig. 8.1, can be treated as two independent shapers that modulate the x- and y-components of electric field separately, before overlaying them interferometrically. For reasons of symmetry, stability, and cost they are integrated in one single shaper setup. First, the incoming beam is split by a beam splitter. The setup is constructed in such a way that the beams enter the grating under different angles but at the same spot, allowing to travel parallel to each other after being collimated by the lens; that way, two regions of the modulator have separate control over the two field components. After re-collimation by the second lens and leaving the second grating, one beam is rotated by 90° by a $\lambda/2$ wave plate, passes through a variable delay, and is then recombined with the second beam in a polarizing beam splitter cube (performing also the amplitude modulation), resulting in almost no intensity loss. As to interferometry involved, the relative phases of the two paths must be stable over time, and a few additional issues have to be considered such as spatial overlap, spectral overlap, temporal overlap, air flow/fluctuations, and temperature equilibrium [28] as they also pass through different parts of the employed components. A good spatial overlap of the two paths can be ensured if

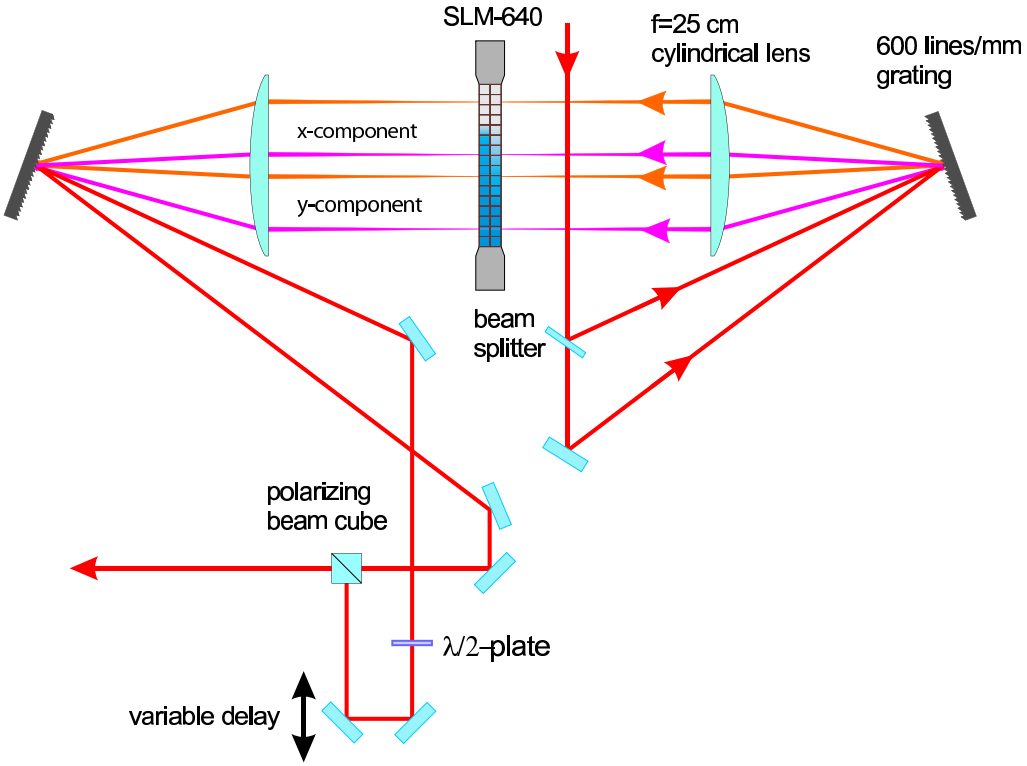

Figure 8.1: Interferometric, "parallel" setup capable of fully controlling phase, amplitude, and polarization of femtosecond pulses.

the same parity of reflecting elements are used for both paths and a wave plate to rotate one beam instead of a periscope. The spectral intensities can be equalized using amplitude modulation (which is multiplied to all further custom amplitude modulations) in order to equalize to two spectral intensity profiles. The temporal overlap is ensured in a two-step way: For a first, course adjustment, the variable delay is shifted while monitoring spectral fringes in a spectrometer; for a fine-tuning, a correction phase mask is applied (which is added to all further phase modulations), constructed using Taylor terms. The linear phase is to fine-tune the temporal overlap with femtosecond precision, a quadratic phase eliminates any residual chirps, and a third order phase (quadratic chirp) corrects for asymmetries in the pulse's rising and falling edges. The zero order phase can be used to compensate for phase drifts caused by temperature changes which induce length variations of the setup's components. They are easily spotted by a change of polarization state, adjusting for such drifts is crucial while performing non-instantaneous measurements, like a cross-correlation. To avoid air fluctuations, air flow, and to keep the temperature stable, the setup is covered by a plastic box. As the electronics of the modulator generate a heat output which varies dependent on data processing, a constant data stream and a continuous triggering of pulse shapes is employed. All measures together yield a thermal equilibrium after about 30 minutes. With all the described arrangements, interferometric stability can be maintained of the order of about 10 minutes, before a slight readjustment of the zero order phase of one component is required.

8.1.2 Output field calculation

A linear combination of two phase- and amplitude modulated, orthogonal components of an electrical field allows for every physically feasible temporal waveform, and can be described by the general filter

$$\tilde{\mathbf{H}}^{par}(\omega) = \begin{bmatrix} R_x(\omega) \cdot e^{i\phi_x(\omega)} \\ R_y(\omega) \cdot e^{i\phi_y(\omega)} \end{bmatrix} \tag{8.1}$$

The output field, depending on the retardances

$$\mathbf{E}_{out}^{par} = E_{in}(\omega) \cdot \underbrace{\begin{bmatrix} e^{\frac{i}{2}[\phi_{ax}(\omega)+\phi_{bx}(\omega)]} \\ e^{\frac{i}{2}[\phi_{ay}(\omega)+\phi_{by}(\omega)]} \end{bmatrix}}_{phase} \cdot \underbrace{\begin{bmatrix} \cos\frac{\phi_{ax}(\omega)-\phi_{bx}(\omega)}{2} \\ \cos\frac{\phi_{ay}(\omega)-\phi_{by}(\omega)}{2} \end{bmatrix}}_{amplitude} = E_{in}(\omega) \cdot \tilde{\mathbf{H}}^{par}(\omega), \tag{8.2}$$

where ϕ_{ax} is the retardance of the x-pass (component) etc.

$E_{in}(\omega)$ (without the factor 1/2 after the beam splitter), is chosen to represent each path's incident pulse in order to keep a consistent nomenclature. The resulting transmissions can be stated as

$$\begin{aligned} T_x(\omega) &= R_x^2(\omega) = \cos^2\tfrac{\phi_{ax}(\omega)-\phi_{bx}(\omega)}{2} \\ T_y(\omega) &= R_y^2(\omega) = \cos^2\tfrac{\phi_{ay}(\omega)-\phi_{by}(\omega)}{2} \end{aligned} \quad . \tag{8.3}$$

The inverse calculation, to provide the retardances necessary to generate a desired output field $\mathbf{E}_{out}$, provides the simple correlation

$$\begin{bmatrix} \tilde{H}_x(\omega) \\ \tilde{H}_y(\omega) \end{bmatrix} = \frac{1}{E_{in}(\omega)} \begin{bmatrix} E_{x,out}^{par}(\omega) \\ E_{y,out}^{par}(\omega) \end{bmatrix}. \tag{8.4}$$

The terms $|\tilde{H}_{x,y}(\omega)|^2$ represent the spectral transmission components $T_{x,y}(\omega)$, to be applied on the modulator for x and y, respectively; and the arguments provide the component's phases as $\phi_{x,y}(\omega) = \arg[\tilde{H}_{x,y}(\omega)]$. As no intensity can be generated by the setup for neither frequency,

$$\int |\tilde{E}_{x,y}(\omega)|^2 d\omega = \int T_{x,y}(\omega) \cdot |\tilde{E}_{in}(\omega)|^2 d\omega \tag{8.5}$$

states the requirement for energy conservation. This also means that the resulting transmissions eventually have to be normalized, by dividing both $T_{x,y}(\omega)$ by the same factor.

8.2 Experimental example pulses

The test pulses are calculated by the same sub pulse parametrization as used in the previous chapter, stated in Eqs. 7.28 to 7.30, which can be directly applied on the modulator. A first test of the parallel setup's temporal shaping capabilities is conducted using the Coherent Mira at λ_0=783 nm and $\Delta\lambda$ = 25 nm in order to generate a Δt =400 fs double pulse with varying polarization states.

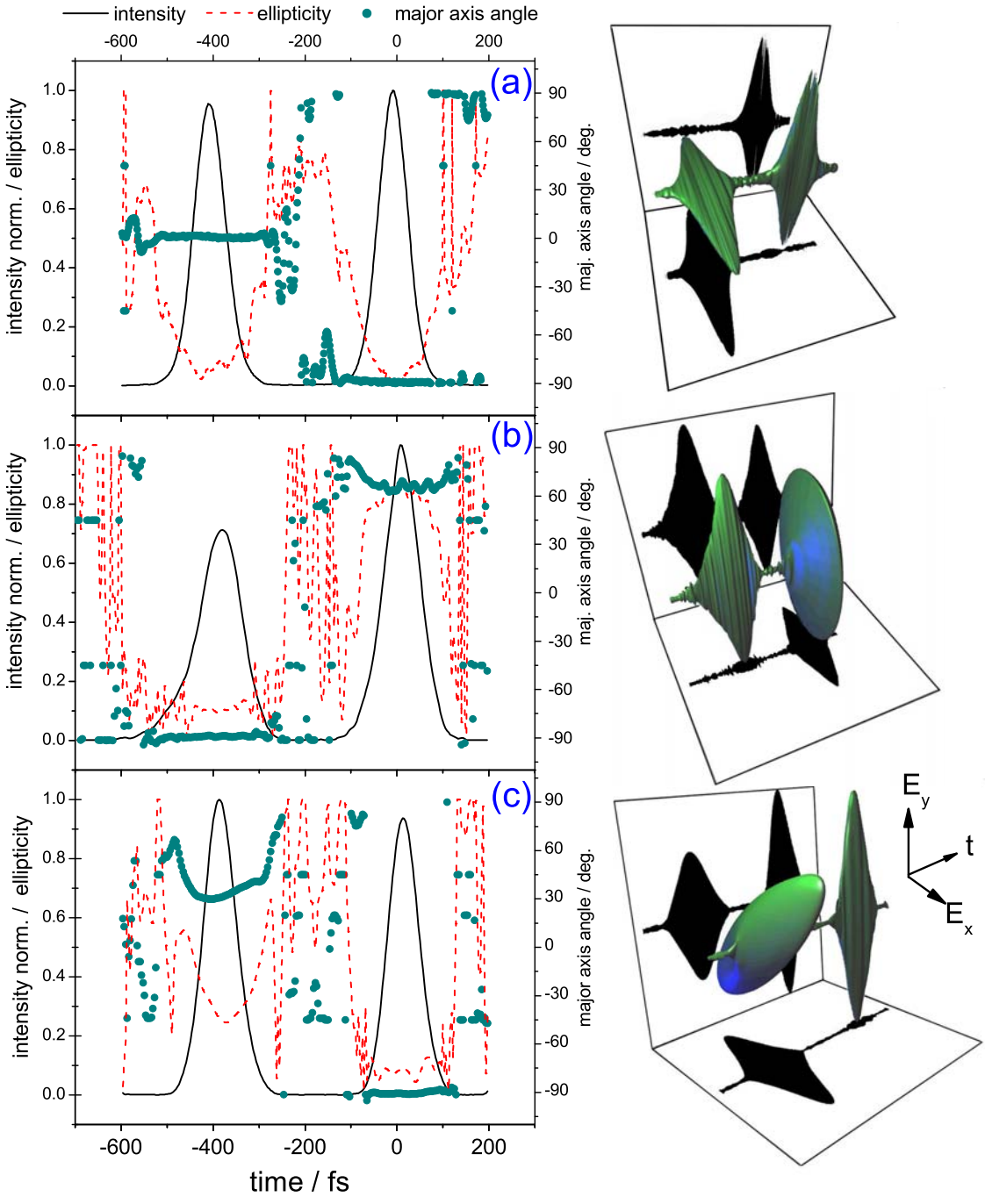

Figure 8.2: Experimental double pulses generated by the parallel setup. (a) Orthogonal, 0°/90° linearly polarized double pulse, (b) linear/circular pulse, (c) elliptical/linear pulse (ellipticity 0.3 and major axis angle 30°). The 3D plots represent the temporal amplitudes of the electric fields.

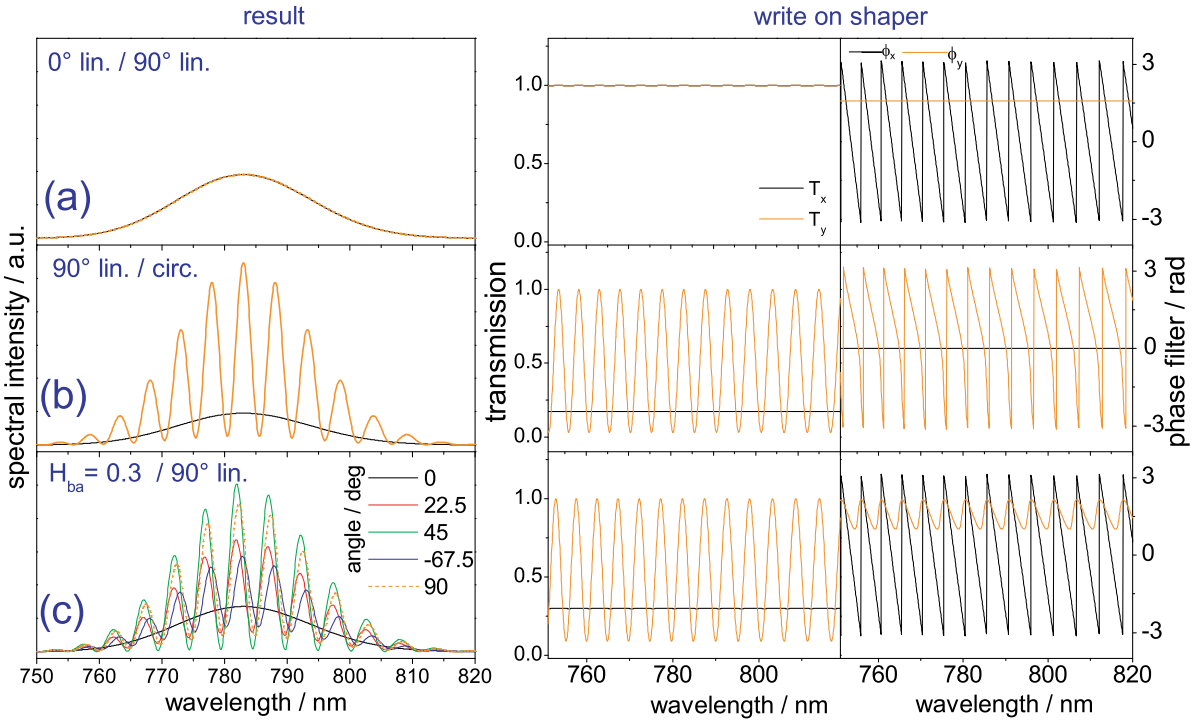

Figure 8.3: Simulated spectra (left column), x- and y-transmissions (middle column), x- and y- phase filter (right column) needed to create the respective experimental pulses (a), (b), and (c) in Fig. 8.2. For (c), a selection of projections to different angles is displayed.

Fig. 8.3 shows applied transmissions (middle column), phases (right column), and resulting spectra (left column) for three example pulses. The corresponding experimental results are presented in Fig. 8.2 as ellipse parameters versus time (left column), and as 3D plot of the temporal amplitude.

Linear/linear. The first example pulse is an orthogonal, 0° and 90° directed, linear double pulse, which requires a constant and equal transmission for both x- and y-directions (Fig. 8.3, middle column), a linear phase in order to shift the x-sub pulse in time, and a flat phase for the y-directed sub pulse, which does not have to be shifted as it is located at t=0 fs (right column). The temporal course of the ellipticity for the sub pulses reaches $H_{ba} < 0.04$ at a minimum (red/ dashed curve in Fig. 8.2 (a)), which is a quite good result, and about the same as the output specifications of the laser system. The angular match to the target is better than 1° for both sub pulses. The noise and frayed edges seen in the 3D representation are due to the TRE-like detection (see Sec. 7.4.1), which yields an increased noise for near-linear states because of the ratio of major/minor axis involved. Destructive interference is utilized successfully when looking at the negligible fraction of x-polarized light for the vertical sub pulse and vice versa.

Linear/circular. Figs. 8.3 and 8.2 (b) portray a linear/circular pulse. Unlike the serial setup, such a pulse form can be created by the parallel setup without side pulses. For the intended circular pulse, an ellipticity of 0.89 could be achieved. The transmission (middle column in Fig. 8.3 (b)) is constant for the x-direction,

as in that plane the y-oriented linear pulse has no component and does not cause interference.

Linear/arbitrary angle, elliptical. The last pulse form (c) consists of an elliptical (at 30°, with a resulting ellipticity of 0.27; 0.33 was intended) and a consecutive linear pulse at 90°. The transmission pattern is similar to the circular case, with a smaller "modulation amplitude"; the crucial difference is the phase filter (right column), which shows that both x- and y-components have to be modulated using different patterns. The resulting spectra, as would appear after a polarizer, are plotted for a few angles, pointing out that there is quite complex information embedded. This particular pulse also can not be generated by the serial setup as here, the major axis angle can be set to 30° without an emergence of side pulses[1] and/or a change to the rest of the waveform.

8.3 Arbitrary temporal fields

If an arbitrary set $\{I(t), H_{ba}(t), \beta(t)/2, hel(t), \varphi(t)\}$ of temporally changing parameters is conceived, it is very well possible that the resulting electrical field is not feasible with a given setup and laser specifications. An analytical study to determine the maximal temporal derivatives of ellipse parameters [138] states (in a condensed way) that the bandwidth of the generating pulse is the most decisive factor for how much the electrical field vector can "twist" and how the "speed limit" on the surface on the Poincaré sphere looks like.

As polarization pulse shaping is also treated in theoretical studies, for example concerning the fabrication of enantiomers which could prefer specific polarization changes over time [156, 157, 158], it would be good to know how temporal polarization profiles from theory (which sometimes have very high demands on bandwidth) would be represented with an experimental, bandwidth-limited laser system. To check how the available bandwidth copes with an arbitrary temporal field, meaning what the reaction of a real-life bandwidth-limited laser system[2] would look like in the time domain, will be discussed next.

8.3.1 Incorporation of a limited laser bandwidth

The procedure is the same as for the previous chapter, where the "response" of the serial setup to an "impossible field" (meaning one it can not generate) was constructed by clipping the imaginary retardances it could not enact.

The steps for such a procedure, starting from constructing a temporal course are illustrated in Fig. 8.4. Using the set transformation equations 7.25 to 7.26, the parameters are first transformed to yield the temporal field $\mathbf{E}_{out}(t) = \hat{x}\ a(t)e^{i\phi_x} + \hat{y}\ b(t)e^{i\phi_y}$. Then, a Fourier transform produces the spectral field $\mathbf{E}_{out}(\omega)$, which

[1] as occurred when attempting to create arbitrary major axis angles with the serial setup as in Fig. 7.17

[2] using an inherently unrestricted polarization pulse shaper such as the parallel setup or an equivalent system, preferably a variant of a four-array liquid crystal modulator, as postulated in [16, 28]

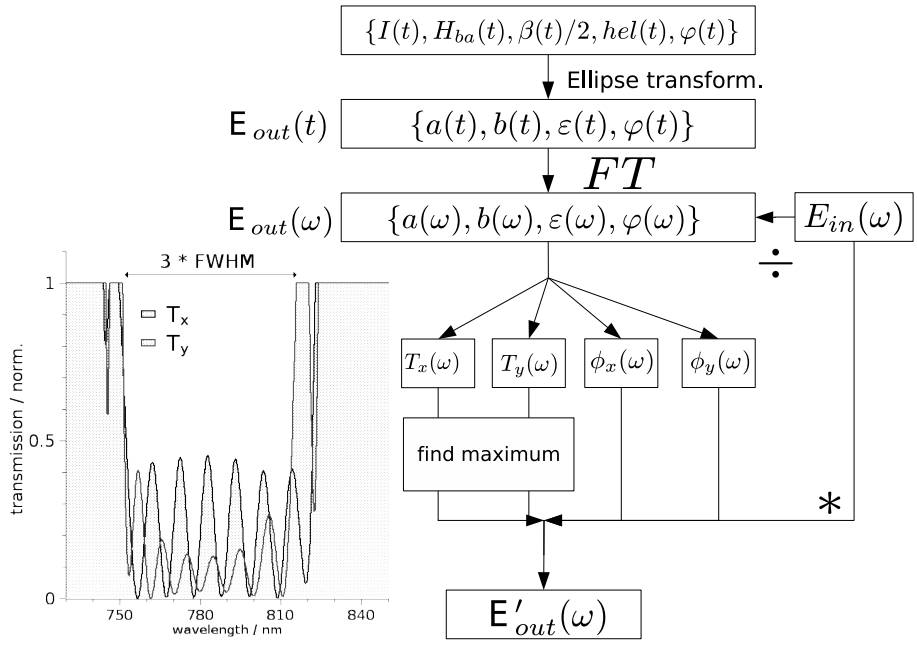

Figure 8.4: Routine limiting an arbitrary field to an experimentally feasible pulse form, using the available bandwidth. The inset on the left depicts the transmission to be applied.

might possess a larger bandwidth than the one available. To determine the shape of an adequate transfer function, it is beneficial to first determine $\mathbf{H}(\omega)$ by dividing the output by the input field as in Eq. 6.12 and inspect the resulting transmissions $T_x(\omega)$ and $T_y(\omega)$ (inset on the left in Fig. 8.4). If the bandwidth is larger than the bandwidth of $E_{in}(\omega)$, the division will result in transmissions that are far greater than one (for wavelengths far off λ_0), which is physically infeasible. An adept normalization, including a cutoff has to depend on the respective shape of $T_{x,y}(\omega)$. If the cutoff/normalization is performed (like in the picture) at the highest value occurring the range of 3×FWHM, the energy loss will be noticeable. When cutting off at lower values, information about the pulse might get lost. After a cutoff is chosen, the input field $E_{in}(\omega)$ can be multiplied back using the new filter function[3], resulting in the physically feasible field $\mathbf{E}'_{out}(\omega)$ for the available laser bandwidth.

8.3.2 Intrapulse modulation

As an example, a simulated Δt=200 fs double pulse[4] with different intra-pulse features will be discussed, and is depicted in Fig. 8.5 (a) as temporal parameter course, as a 3D graph of the temporal amplitude in (b) and as extended Poincaré representation in (c).

The first sub pulse at t= -200 fs is constructed with a Gaussian intensity profile, a major axis angle of 40°, and an ellipticity of 0.3. Now, a very fast helicity swap from left to right handed is introduced, from one sampling point to the next (δt =1.33 fs), displayed by the small black bars on the bottom of (a). The right-circular part of this pulse can also be seen in the extended Poincaré representation (c), where the

[3]with no change to the phases
[4]with a bandwidth of $\Delta\lambda$ =25 nm FWHM

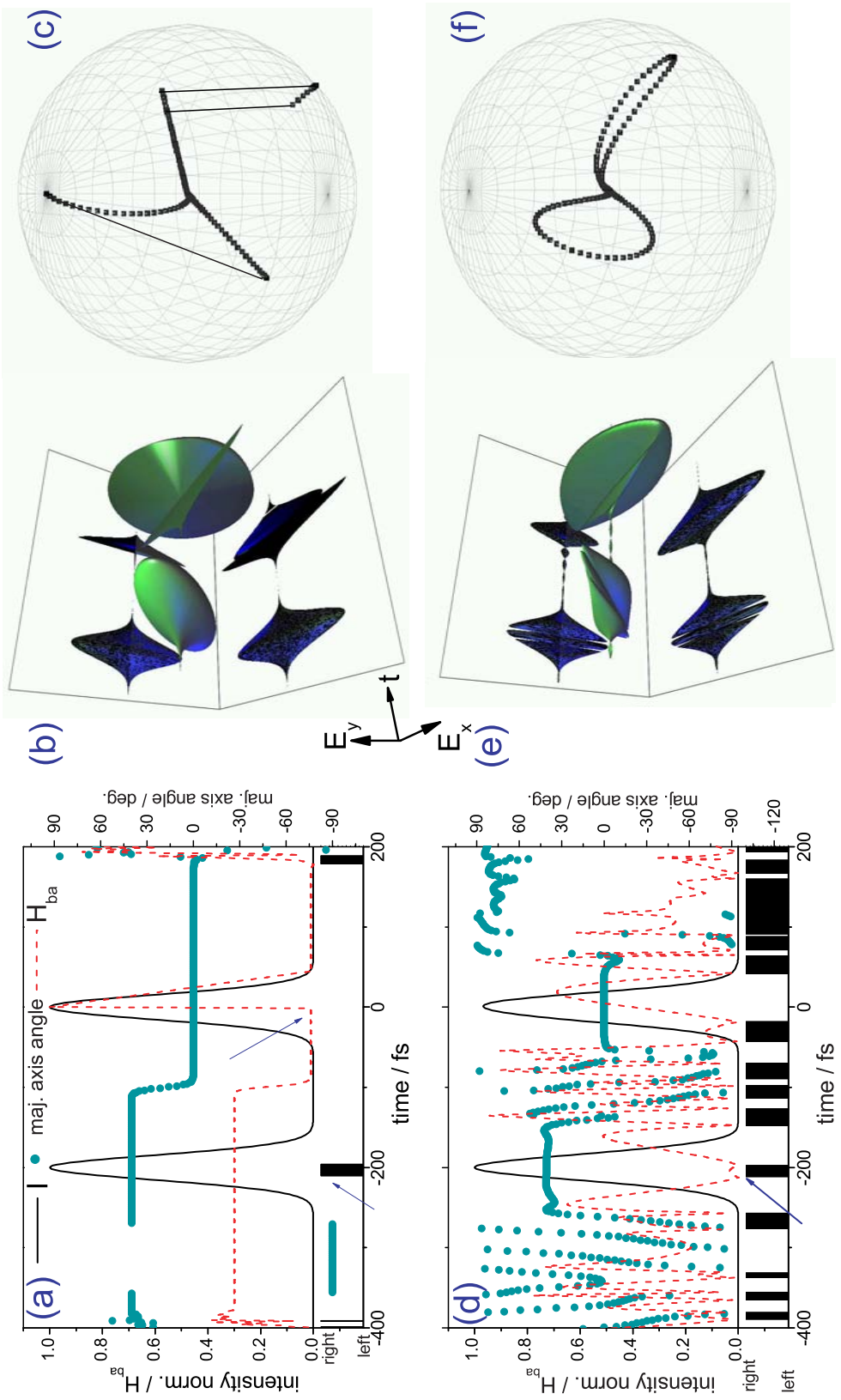

Figure 8.5: Arbitrary temporal pulse form with a higher-than-available bandwidth requirement. In (a) the simulated temporal course of the ellipse parameters is shown, in (b) the 3D representation of the temporal amplitude, and in (c) the extended Poincaré representation. Figures (d)-(f) depict the response of a 25 nm FWHM laser system to input from (a)-(c).

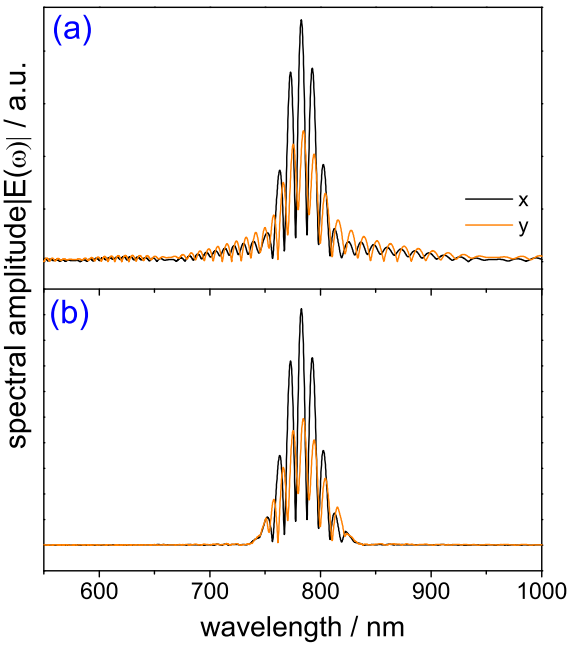

Figure 8.6: (a) Spectrum for the arbitrary temporal profile shown in Fig. 8.5 (a)-(c). Graph (b) displays the bandwidth-restricted spectrum (FWHM of 25 nm) from Fig. 8.5 (d)-(f).

path suddenly jumps to the southern hemisphere. The second sub pulse at t=0 fs features an instantaneous ellipticity change from linear to circular, seen as a sharp edge in H_{ba} in (a) (see arrow), similarly in the 3D representation (b), and symbolized as straight[5] connection line between equator and north pole in (c).

With the above described steps (Fig. 8.4), the response of a laser with a finite bandwith to the intrapulse insets can be calculated. The spectral amplitudes $|E_{out}|_{x,y}$ of the pulse form including the desired intra-pulse modulations are plotted in Fig. 8.6 (a). In (b), the resulting spectral amplitudes when the transmission clipping (inset in Fig. 8.4) is applied, is shown. The effect of the restriction in the time domain is visualized in Fig. 8.5 (d)-(f). The t=-200 fs sub pulse's requirement for a very fast helicity change causes the left-handed ellipticity of 0.3 to gradually change to linear, as only then, the helicity change can be accomplished. Afterwards, it tries to reach the right-handed original value of 0.3, but is interrupted soon as it has to (symmetrically) return to the original value. As a result, only a small right-circular "dip" (marked by an arrow in the graph) which is symmetrically surrounded by a symmetrical, steep ellipticity change of $dH_{ba}/dt = (\pm 0.020 \pm 0.003)$ fs^{-1} with nearly no effect to the major axis angle is observed. The "dip" can also be seen in the 3D representation (e) which shows two "incisions"[6] to the originally uniform elliptical pulse and in (f), where the disconnected tail becomes connected.

The second sub pulse at t=0 fs with the required very fast (δt = 1.33 fs) change from linear to circular shows a steep ellipticity change (d) from the original linear,

[5]which originates from the employed data sampling; with a higher sampling it would become a path on the surface as the intensity stays unchanged at the cut

[6]Such incisions were also discussed in Ref. [159] for their potential use in high-order harmonic generation and attosecond generation.

but only to elliptical - and not circular as intended, see (e) - as there is not enough time (or high enough frequencies contained in the input spectrum) to reach it. The electrical field can only change as much as the highest frequencies contained in the broadband spectrum it is composed of, again demonstrating that the maximal speed for a temporal change is determined by the original bandwidth[7]. In (f), the before abruptly changing paths are now all interconnected smoothly with a reduced maximal curvature.

8.4 Summary and Outlook

In this chapter, the possibilities of an inherent restriction-free polarization pulse setup, such as the interferometric, parallel setup are described in the time domain and the first experimental custom-tailored, parametric pulse forms with arbitrary major axes without side-effects are shown. The example pulses correspond well to the desired shapes and show no degradation in comparison with the single pulse tests [21]. The method of generating the pulses, unfortunately, only allows for the pulse forms to be stable for a matter of a few minutes before (small) readjustments are required; making prolonged experiments, as for example molecular beam experiments with an evolutionary algorithm difficult for the time being. This could be overcome with an active stabilization which keeps the phase-lock between the x- and y-component, experimentally realized with a piezo element coupled to the beam combiner's leakage. A faster detection could be realized by a vibrating element that changes length on a scale corresponding to a few picoseconds (of the order of a few millimeters) at the delay, allowing to perform a very fast pulse acquisition. An active temperature regulation circuit/element would also help eliminating the phase drifts, enabling the parallel setup to be fully utilized for coherent control studies. Particularly, an arbitrary control over major axis angle plus the side pulse-free pulse generation could be useful for systematically investigating more complex molecules that feature non-orthogonal dipole moments.

The presented routine reviewing the feasibility of a bandwidth-limited laser system to produce arbitrarily shaped polarization transient could be of interest if pulse forms requiring higher bandwidths, for example originating from theoretical studies, are to be generated. A routine to find viable compromises could maybe even be automated in a sense that a concession between the individual ellipse parameters is to be found by an iterative algorithm, or even manually, like a "pulse painter".

[7] as derived in [138]